GaAs Infrared Detectors

S. D. Gunapala, and S. V. Bandara

Center for Space Microelectronics '1'ethnology, Jet Propulsion Laboratory,
California Institute of I'ethnology, Pasadena, CA 91109

A. Introduction

It is customary to make infrared (IR) detectors in the long wavelength range (8 -20 pm) by utilizing the interband transition which promotes an electron across the band gap (E_g) from the valence band to the conduction. These photo-electrons can be collected efficiently, thereby producing a photocurrent in the external circuit. Since the incoming photon has to promote an electron from the valence band m the conduction band, the energy of the photon (hv) must be higher than the E_g of the photosensitive material. Therefore, the spectral response of the detectors can be controlled by controlling the E_g of the photosensitive material and detection of very long wavelength IR radiation up to 20 um requires small band gaps down to 62 meV. Examples of such materials meeting these requirements are $Hg_{1-x}Cd_xTe$ and $Pb_{1-x}Sn_xTe$ in which the energy gap can be controlled by varying x. It is well known that these low band gap materials art more difficult to grow and process than large band gap semiconductors such as GaAs. These difficulties motivate the exploration of utilizing the intersubband transitions in multi quantum well (MQW) structures made of large band gap semiconductors[1-8] (see Fig. 1).

B. Quantum Well Infrared Photodetectors

A MQW structure designed to detect infrared (IR) light is called a quantum well infrared photodetector (QWIP). An elegant candidate for QWIP is the square quantum

wcll of basic quantum mechanics.[9] When the quantum well is sufficiently deep and narrow, its energy states are quantized (discrete). The potential depth and width of the well can be adjusted so that it holds only two energy states: a ground state near the well bottom, and a first excited state near the well top. A photon striking the wc]] will excite an electron from the ground state to the first excited state, then an externally-applied voltage sweeps it out producing a photocurrent (Fig. 1). Only photons having energies corresponding to the energy separation between the two states are absorbed, resulting in a detector with a sharp absorption spectrum. Designing a quantum well to detect light of a particular wavelength becomes a simple matter of tailoring the potential depth anti width of the well to produce two states separated by the desired photon energy. The $GaAs/Al_xGa_{1-x}As$ material system allows the quantum well shape to be tweaked over a range wide enough to enable light detection at wavelengths longer than - 6 μm.[10-11] Fabricated entirely from large bandgap materials which are easy to grow and process, it is now possible to obtain large uniform FPAs of QWIPs tuned to detect light at wavelengths from 6 to 25 μm in the $GaAs/Al_xGa_{1-x}As$ material system. [12-16]

Currently, there is a great interest in the $GaAs/Al_xGa_{1-x}As$ based QWIP due to its higher sensitivity, higher uniformity, higher yield, and lower cost. Therefore, in this section **24.5, wc** are focusing most of our attention On $GaAs/Al_xGa_{1-x}As$ based QWIPs. Typically each period of the multi-quantum well (MQW) structure consists of a 30- 1 ()() Å well of GaAs (doped n = 1×10^{18} cm^{-3}) and a 500 Å barrier of $Al_xGa_{1-x}As$. [10] " Stacking many identical quantum wells (typically 50) together increases photon absorption. Ground state electrons arc provided in the detector by doping the GaAs well layers with Si. This photosensitive MQW structure is sandwiched between 0.5 μm GaAs top and bottom contact layers doped n = 1×10^{18} cm^{-3}, grown On a semi-insulating GaAs substrate by molecular beam epitaxy (MBE). Then a GaAs cap layer about 1 μm thick was grown in *situ on* top of the photosensitive MQW layers to fabricate the light coupling optical cavity.

C. 'roperties of QWIP

c1.)ark Current

improving QWIP performance depends largely on minimizing the parasitic current that plagues all light detectors, the dark current (the current that flows through a biased detector in the dark, i.e., with no photons impinging on it). In QWIPs, the dark current originates from three different mechanisms. [17-21] As shown in Fig. 1, the dark current arising from the first process is clue to quantum mechanical tunneling from well to well through the $Al_xGa_{1-x}As$ barriers (sequential tunneling). 'l'his process is independent of temperature. Sequential tunneling dominates the dark current at very low temperatures (<30 K). The second mechanism is thermally assisted tunneling which involves a thermal excitation and tunneling through the tip of the barrier into the continuum energy levels. This process governs the dark current at medium temperatures. The third mechanism is classical thermionic emission and it dominates the dark current at higher temperatures (>55 K for 9 μm cutoff QWIPs). The thermal generation rate associated with this current depends on the well doping density and the life time of the carriers which will be determined by the thickness of the AlxGa1-xAs barriers.[22] Consequently, for QWIPs operating at higher temperatures the last mechanism is the major so urce of dark current[16,17]

The best previous QWIPs (pioneered by Barry Levine *et al.* [6] at AT&T Bell Labs) were of the bound-to-continuum variety, so-called because the first excited state was a continuum energy band above the well top (typically 10 meV). Later, Gunapala *et al.* designee] the *bound-to- quasibound* quantum well by placing the first excited state exactly at the well top as shown in Fig. 2. Dropping the first excited state to the well top causes the barrier to thermionic emission (roughly the energy height from the ground state to the wc]] top) to be - 10 meV more in *bound-to-quasibound* QWIP than in the bound-to-continuum one, theoretically causing the dark current to drop by a factor of - 6 at a temperature of 70 K. [16] The dark current-voltage curve of the 8.5 μm peaked bound-to-quasibound QWIP is shown in Fig. 2. This compares well with the experimentally

observed factor of -4 drop compare to the *bound-to-cont inuum* QWIP having the same peak wavelength.

C2. Responsivity

Typical responsivity spectrums of bound-to-bound, bound-to-continu um, and bound-to-quasibound QWIPs are shown in Fig. 3. Unlike the responsivity spectrums of intrinsic infrared detectors, the responsivity spectrums of QWIPs are much narrow and sharper due to their resonance intersubband absorption. 'I'he normalized responsivity spectra R (λ) are given in Fig. 3 for samples A-F, where we see that the *bound* and *quasibound* excited state QWIPs (samples E and F) arc much narrower $\Delta\lambda/\lambda$ = 1()%-11 % than the *continuum* QWIPs $\Delta\lambda/\lambda$ = 19%-28% (samples A-D). Table I gives the responsivity peak λ_p and cutoff wavelengths λ_c as well as the responsivity spectral width $\Delta\lambda$.

The absolute peak responsivity R_p can be written in terms of quantum efficiency η and photoconductive gain g as

$$R_p = (e/h\nu)\,\eta\, g. \qquad (1)$$

The bias dependence of R_p is shown in Fig. 4. Note that at low bias the responsivity is nearly linearly dependent on bias and it saturates at high bias. This saturation occurs due to the saturation of carrier drift velocity. For the longest wavelength sample D, where λ_c = 19 pm, the dark current becomes too large at high bias to observe the saturation in R_p. The responsivity of *quasibound* QW1 P (sample F) behaves quite similarly to the *continuum* QWIPs of Fig. 4, the fully *bound* sample E has a significantly different shape. The responsivity does not start out linearly with bias but is in fact zero for finite bias. That is, there is a zero bias offset of more than 1 V, due to the necessity of field assisted tunneling for the photoexcited carrier to escape from the well [5, 23-25]

C3. Detector noise

The dark current noise (Shott noise) for sample B at temperature T=77 is shown in Fig. 5. The solid circles were measured for negative bias (mesa top negative) while the open circles were measured for positive bias. "The smooth curves have been drawn through the experimental data. Note that the current shot noise for positive bias is much larger than that for negative bias (e. g., at $V_b = 3.5$ V it is 4 times larger), and also that near $V_b = 4$ V there is a sudden increase in the noise due to a different mechanism (possibly due to the avalanche gain [25] process). 'This asymmetry in the dark current noise is clue to the asymmetry in the dark current for positive and negative bias voltages. [20] The photoconductive gain g can now be obtained using the current shot noise expression [17, 19, 27]

$$i_n = \sqrt{4eI_d g\Delta f}\,, \tag{2}$$

where Δf is the band width, (taken as $\Delta f = 1$ Hz). This expression is valid for small quantum well capture probabilities (i.e., $p_c<<1$). QWIPs satisfy this condition at usual operating bias (i. e., 2-3 V). There were many studies [28-30] on the optical and electrical gain anti relationship between gain and noise properties of QWIPs. A more general formula [29] which can apply even in low bias conditions where well capture probabilities are high is given by $i_n^2 = 4eI_d g\Delta f(1 - p_c/2)$.

C4. Detectivity

Detectivity D^* is a commonly used figure of merit and it is defined as [17,19]

$$D^* = R\frac{\sqrt{A\Delta f}}{i_n} \tag{3}$$

where A is the detector area and Af = 1 Hz. This is done as a function of bias for a *continuum* (A), a *bound* (E), and a *quasibound* (F) QWIP in Fig. 6. (The dashed lines near the origin are extrapolations.) For all three samples D^* has a maximum value at a bias between V_b = -2 to -3 V. Since these QWIPs all have different cutoff wavelengths, these maximum D^* values cannot be simply compared. The primary noise source in QWIPs is the shot noise produced by the dark current. '] 'Hereford, unlike the narrow band gap detectors in which the noise is dominated by temperature independent processes at low temperatures, QWIP performance can be further improved by cooling to cryogenic temperatures. [10]

D). Light Coupling

QWIPs do not absorb radiation incident normal to the surface since the light polarization must have an electric field component normal to the superlattice (growth direction) to be absorbed by the confined carriers. When the incoming light contains no polarization component along the growth direction the matrix element of the interaction vanishes (i. e.. $\vec{\varepsilon}.\vec{p}_z=0$ where $\vec{\varepsilon}$ is the polarization and $\vec{p}_z$ is the momentum along 7 direction). As a consequence., these detectors have to be illuminated through a 45" polished facet [10]. Clearly, this illumination scheme limits the configuration of detectors to linear' arrays and single elements. For imaging, it is necessary to be able to couple light uniformly to two dimensional arrays of these detectors. Several monolithic grating structures [3,"3'] have been demonstrated for efficient light coupling to a QWIPs. and it made two dimensional QWIP imaging arrays feasible. It has been shown that many more passes of IR light, and significantly higher absorption, can be achieved with a randomly roughened reflecting surface. [36] By careful design of surface texture randomization, a factor-of-eight enhancement in responsivity compared to 45° illumination was demonstrated experimentally. [36] Naturally, thinning down the substrate enables more bounces of light and therefore higher responsivity. One of the main differences between the effect of the cross grating and the random reflector is the shape of the responsivity

curve; unlike the cross grating, the random reflector has little impact on the bandwidth of the response curve since the scattering efficiency of the random reflector is significantly less wavelength dependent than for the regular grating. Therefore, for QWIPs with random reflectors the integrated responsivity is enhanced by nearly the same amount as the peak responsivity.

E. Imaging Arrays

After the grating or random reflector array was defined by the lithography and dry etching, the photoconductive QWIP pixels of a large focal plane array (FPA) (i.e., 256x256 or larger) can be fabricated by wc(or dry etching through the photosensitive GaAs/$Al_xGa_{1-x}As$ MQW layers into the doped GaAs bottom contact layer. Typical pixel-to-pixel distance (i.e., pitch) of these large area FPAs varies from 30 to 50 μm. The random reflectors or gratings on top of the detectors were then covered with Au/Ge and Au for Ohmic contact and reflection. Figure 7 shows twenty five processed QWIP FPAs on a 3 inch GaAs wafer. Iridium bumps were then evaporated on top of the detectors for Si readout circuit hybridization. Then these QWIP FPAs hybridized (via iridium bump-bonding process) to silicon CMOS readout multiplexers to yield the final imaging FPA units. At temperatures below 72 K, the signal to noise ratio of the QWIP FPAs are limited by array non-uniformity, multiplexer readout noise, and photo current (photon flux) noise. At temperatures above 72 K, temporal noise due to the QWIP's higher dark current becomes the limitation. As mentioned earlier this higher dark current is due to thermionic emission and thus causes the charge storage capacitors of the readout circuitry to saturate. Since the QWIP is a high impedance device, it should yield a very high charge injection coupling efficiency into the integration capacitor of the multiplexer, In fact charge injection efficiencies approaching 90% have been demonstrated.[12, '(']

These FPAs were back-illuminated through the flat thinned substrate membrane (thickness ≈ 1300 Å). These QWIP FPAs gave excellent images with 99.98% of the pixels working (number of dead pixels ≈ 1 ()) , demonstrating the high yield of GaAs technology.[15-16] The operability was defined as the percentage of pixels having noise

equivalent differential temperature less than 100 mK at 300" K background and usual operability of GaAs based QWIP FPAs closely agrees with the pixel yield. Figure 8 shows a typical noise equivalent differential temperature (NEΔT) histogram of a QWIP FPA at an operating temperature of T = 70 K at 300 K background and the mean value is 26 mK. " '] 'ypical uncorrected photocurrent non-uniformit y of a large area QWIP FPA is about 5% (= sigma/mean). [16] The non-uniformity after two-point (17 ^{0} and 27 ^{0} Celsius) correction improves to an impressive ().05%. As mentioned earlier, this high yield is due to the excellent GaAs growth uniformity and the mature GaAs processing technology,

F. Other types of MQW IR detectors

F1. Miniband transport multi quantum well infrared detector

The miniband transport (MBT) IR detector, which is functionally equivalent to the bound-to-miniband design,[37] uses doped GaAs quantum well containing two bound states separated by short period AlxGa1-xAs superlattice barrier layers. The quantum wells arc designed such that the higher energy level is resonant with the ground state miniband in the superlattice barrier. The in frared radiation is absorbed in the doped quantum wells, exciting an electron which is transported in the miniband and generates photocurrent. The structure parameters of the quantum well (well width and barrier height) have some flexibility because it is possible to obtain the same operating wavelength with a continuous range of well widths and barrier heights.[14,38] The performances of 128x128 and 256x256 FPAs based on GaAs/Al_xGa_{1-x}AS MBT MQW demonstrates that these are very competitive with the other LWIR technologies. The detectors typically have peak wavelength of 9.1 µm and spectral band width 1.2 mm shows peak D* 2x1 0^{10} cm $Hz^{1/2}$/W at 77K. The temporal and fixed pattern NEΔT of 15 mK and 30 mK respectively have been reported on these FPAs operating at 60K.

F2. **Infrared** hot electron transistor

The infrared hot electron transistor (11111'1')3' is an infrared sensitive three terminal device which utilizes an IR sensitive GaAs/AlGaAs multi quantum well structure as emitter, a wide (1500 A) GaAs layer as base, and a thick quantum barrier placed in front of the collector as an electron energy high pass filter. The energy filter is designed to selectively filter higher energy electrons (mostly photocurrent) to the collector and to reject lower energy electrons (mostly dark current) which are drained through the base. in general, an IHET can be considered as a two-stage device, in which each stage has a unique function. The emitter stage is designed to give desirable optical properties, and collector stage is designed to improve its electrical properties. By using a InGaAs instead of a GaAs layer as a base layer, at 77K, D* of 1.4x101D cmHz$^{1/2}$/W for a device. with cut-off wavelength 9.5 μm has been reported[40]. In addition to reduction of dark cm-rent. these devices are expected [0 reduce readout noise due to their large output impedance. Although substantial research has been carried out on these IHET devices, a FPA or an infrared imager based is yet to be demonstrated.

F3. p-Doped QWIPs

in all the work discussed in this chapter the quantum wells were doped with electrons(n-type). For these n-doped GaAs quantum wells the quantum mechanical selection rule forbids normal incident absorption (Section D). For p-doped QWIPs, however the strong mixing between the light anti heavy holes in the valence band permits normal-incidence absorption. in order to take maximum advantage of this, the GaAs quantum wells have to be doped heavily (typically 4x1 ()]* cm ^{3} with Be). A normal incidence quantum efficiency of 28% and defectivity of D*= 3x10^{10} cmHz$^{1/2}$/W at T=77K, for cutoff wavelength 7.9 pm, have been achieved for bound-to-continuum p-type QWIPs.[41] 1(is worth noting, optical gain of p-type QWIPs is over one order of

magnitude smaller than the corresponding val ue for n-type QWIPs due to the lower carrier velocity associated with higher hole effective. mass.

G. Conclusion

The basic advantages of the GaAs based .WIR detectors, namely the highly mature GaAs growth and processing technologies, become more important at longer wavelengths where the narrow band gap materials becomes more difficult to work with. Exceptionally rapid progress has been made in the performance (i.e., detectivity, N}{ AT, minimum resolvable temperature. difference, uniformity, etc.) of long wavelength QWIPs (i.e., 6-25 pm), starting with bound-to-bound QWIPs which had relatively poor sensitivity, and culminating in high performance *bound-to-qu asibound* QWI Ps. Extremely good progress has been reported in light coupling schemes starting from 45 " polished face to efficient cross gratings and random reflectors. Detectivities higher than 1 $x10^{11}$ $cmHz^{1/2}/W$ have been achieved with 8-10 μm <)WII's at **77** K and 13-15 μm QWIPs at 50 K. '] 'hese operating temperatures can be easily achieved by single stage Stirling coolers. Due to this high performance and the excellent uniformity of GaAs based QWIPs, several groups [12-16] have demonstrated IR imaging cameras based on large (two dimensional array of 128x1 28, 256x256, and 640x480 pixels) QWIP arrays up to a cut off wavelength of 15 μm. Due to the availability of large area FP As, easy manufacturabilit y, high internal impedance, low 1/f noise, high radiation hardness, low cost (i.e.., high yield), easy hybridization to readout electronics, and high uniformity of QWIP, it is a potential candidate variety of ground- based and space-based I R applications.

Acknowledgments
The research described in this article was performed partly by the Center for Space Microelectronics Technology, J e t Propulsion Laboratory, California Institute of '1'ethnology, and was partly sponsored by the National Aeronautics and Space Administration, office. of Advanced Concepts and Technology.

G. References

1. L.Esaki and H.Sakaki, IBM Tech.Disc.Bull. 20, 2456 (1977).
2. J. S. Smith, L. C. Chiu, S. Margalit, A. Yariv, and A. Y. Cho, J. Vat. Sci. Technol. B 1, 376 (1983),
3. D. D. Coon and R. P. G. Karunasiri, Appl. Phys. Lett. 4S, 649 (1984).
4. L. C. West and S. J. Eglash, Appl. Phys. Lett. 46, 1156 (1985).
5. B. F. Levine, K. K. Choi, C. G. Bethea, J. Walker, and R. J. Malik, Appl. Phys. Lett., SO, 1092 (1987).
6. B. F. Levine, C. G. Bethea, G. Hasnain, J. Walker, and R. J. Malik, Appl. Phys. Lett., 53,296 (1988).
7. D. D. Coon and K. M. S. V. Bandara, in *Physics of Thin Films*, edited by M, H. Francombe and J. L. Vossen, Academic, NY, 1991, Vol. 15.
8. K. K. Choi, J. Appl. Phys. 73, 5230 (1993).
9. C. Weisbuch, in *Semiconductors and Semimetals*, edited by R. Dingle, Vol. 24, pp. 1-133, Academic Press, NY, 1987.
10. S. D. Gunapala anti K. M. S. V. Bandara, in *Physics of Thin Films*, edited by M. H. Francombe and J. L. Vossen, vol. 21, pp. 113-237. Academic Press, NY, 1995.
11. B. F. Levine, J. Appl. Phys. 74, R1 (1993).
12. C. G. Bethea, B. F. Levine, M. "1'. Asom, R. E. Leibenguth, J. W. Stayt, K. G. Glogovsky, R. A. Morgan, J. Blackwell, and W. Parrish, IEEE Trans. Electron. Devices 40 (Nov. 1993).
13. L. J. Kozlowski, G. M. Williams, G. J. Sullivan, C, W. Farley, R. J. Andersson, J. Chen, D. 'I'. Cheung, W. E. Tennant, and R. E. DeWames, IEEE Trans. Electron. Devices **ED-38**, 1124 (1991).
14. W. A. Beck, T. S. Faska, J. W. Little, J, Albritton, and M. Sensiper, Second International Symposium on 2-20 μm Wavelength infrared Detectors and Arrays: Physics and Applications, October 10-12, 1994, Miami Beach, Florida.
15. S. D. Gunapala, J. S. Park, G. Sarusi, 1. 1,. Lin, J. K. Liu, P. D. Maker, R. E. Muller, C. A. Shott, '1'. Hoelter, and B. F. Levine "128x128 GaAs/AlGaAs QWIP

FocalPlane Array for Imaging at15 pnl''-Acccpted for publication on IEEE Transactions on Electron Devices.

S. D. Gunapala, J. S. Park, G. Sarusi, 'T'. L. Lin, J. K. Liu, P. D. Maker, R. E. Muller, C. A. Shott, '1'. Hoelter, and B. F. Levine, "9µm Cutoff 256X256 GaAs/$Al_xGa_{1-x}As$ Quantum WC]] Infrared Photodetector Hand-held Camera", Accepted for publication on IEEE Transactions on Electron Devices.

B. F. Levine, C. G. Bethea, G. Hasnain, V. O. Shen, E. Pelve, R. R. Abbott, and S. J. Hsieh, Appl. Phys. Lett., S6, 851 (1990).

S. D. Gunapala, B. F. Levine, 1,. Pfeiffer, and K. West, J. Appl. Phys. 69, 6517 (1990).

A. Zussman, B. F. Levine, J. M. Kuo, and J. de Jong, J. Appl. Phys. 70. 5101 (1991).

E. Pelve, F. Beltram, C. G. Bethea, B. F. Levine, V. O. Shen, S. J. Hsieh, R. R. Abbott, J. Appl. Phys. 66,5656 (1989).

M. A. Kinch and A. Yariv, Appl. Phys. Lett. **55**, 2093 (19S9).

E. Rosencher, F. Luc, P. Bois, J. Nagle ans Y. Cordier, Appl. Phys. Lett., 63, 3312 (1993)

B. F. Levine, C. G. Bethea, K. K. Choi, J. Walker, and R. J. Malik, Appl. Phys. Lett. 53, 231 *(1987).*

K. K. Choi, B. F. Levine, C. G. Bethea, J. Walker, and R. J. Malik, Phys. Rev. Lett. **59**, 2459 (1987).

N. Vodjdani, B. Vinter, V. Berger, E. Bockenhoff, and E. Costard, Appl. Phys. Lett. **59**, 555 (1991).

B. F. Levine, K. K. Choi, C. G. Bethea, J. Walker, and R, J. Malik, Appl. Phys. Lett., 51,934 (1987).

G. Hasnain, B. F. Levine, S. Gunapala, and N. Chand, Appl. Phys. Lett. **57**, 608 (1 990).

H. C. Liu, Appl. Phys. Lett. 61, 2703 (1992).

W. A. Beck, Appl. Phys. Lett. 63, 3589 (1993).

K. K. Choi, Appl. Phys. Lett. **65**, 1266 (1994)

31. K. W. Goosen and S. A. Lyon, Appl. Phys. Lett. 47, 1257 (1985).

32. G. Hasnain, B. F. Levine, C. G. Bethea, R. A. Logan, J. Walker, and R. J. Malik, Appl. Phys. Lett. 54, 2515 (1989).

33. J. Y. Andersson, L. Lundqvist, and Z. F. Paska, Appl. Phys. Lett. **58**, 2264 *(1991).*

34. J. Y. Andersson and L. Lundqvist, Appl. Phys. Lett. **59**, 857 (1991).

35. J. Y. Andersson, L. Lundqvist, and Z. F. Paska, J. Appl. Phys. 71, 3600 (1991).

36. G. Sarusi, B. F. Levine, S. J. Pearton, K. M. S. V. Bandara, and R. E. Leibenguth, Appl. Phys. Lett. 64,960 (1994)

37. L. S. Yu and S. S. Li, Appl. Phys. Lett. S9, 1332 (1991).

38. W. A. Beck, J. W. Little, A. C. Goldberg, and T. S. Faska, in Quantum Well Intersubband Transition Physics and Devices, edt by H. C. Liu, B. F. Levine, and J. Y. Andersson, pp. 55-68, Kluwer Academic, Netherlands (1993).

39. K. K. Choi, M. Dutta, P. G. Newman, and M.-L. Saunders, Appl. Phys. Lett. **57**, 1348 (1990).

40. K. K. Choi, L. Fotiadis, M. Taysing-Lara, and W. Chang, Appl. Phys. Lett. **59**, 3303 (1991).

41. B. F. Levine, S. D. Gunapala, J. M. Kuo, S. S. Pei, and S. Hui, Appl. Phys. Lett. **59**, 1864(1991)

Figure Captions

Fig. 1 Schematic diagram of the conduction band in a bound-to-quasibound QWIP in an externally applied electric field. Absorption of IR photons can photoexcite electrons from the ground state of the quantum well into the continuum, causing a photocurrent. Three dark current mechanisms are also shown: ground state tunneling (1); thermally assisted tunneling (2); and thermionic emission (3). The inset shows a cross-section transmission electron micrograph of a QWIP sample.

Fig. 2 Comparison of dark currents of bound-to-continuum and bound- to-quasibound QWIPs as a function of bias voltage at temperature $T = 55$ K.

Fig. 3 Normalized responsivity spectra Vs wavelength measured at $T = 20$ K for samples A-F.

Fig. 4 Bias dependent peak ($\lambda = \lambda_p$) responsivity R_p^0 measured at $T = 20$ K for samples A-D. The insert shows the conduction band diagram.

Fig. 5 Dark current noise i_n (at $T = 77$ K) Vs bias voltage V_b for sample B. Both positive (open circles) and negative (solid circles) bias are shown. The smooth curves are drawn through the measured data. The insert shows the conduction band diagram.

Fig. 6 Detectivity D^* (at $T = 77$ K) Vs bias voltage V_b for samples A. E and F. The inserts show the conduction band diagram.

Fig. 7 Twenty five 256x256 QWIP focal plane arrays or a 3 in. GaAs wafer.

Fig. 8 Photosignal histogram of the 65,536 pixels of he 256x256 array showing a high uniformity of the FPA. The uncorrected non-uniformity (= standard deviation/mean) of the FPA is only 6.8% including 1% non-uniformity of ROC and 1.4% non

uniformity due to the cold-stop not being able to give the same field of view m all the pixels in the FPA.

Tables

1. Responsivity and spectral parameters for samples A-F, including peak responsivity wavelength λ_p, long wavelength cutoff λ_c, spectral width $\Delta\lambda$, and fractional spectral width $\Delta\lambda/\lambda$.

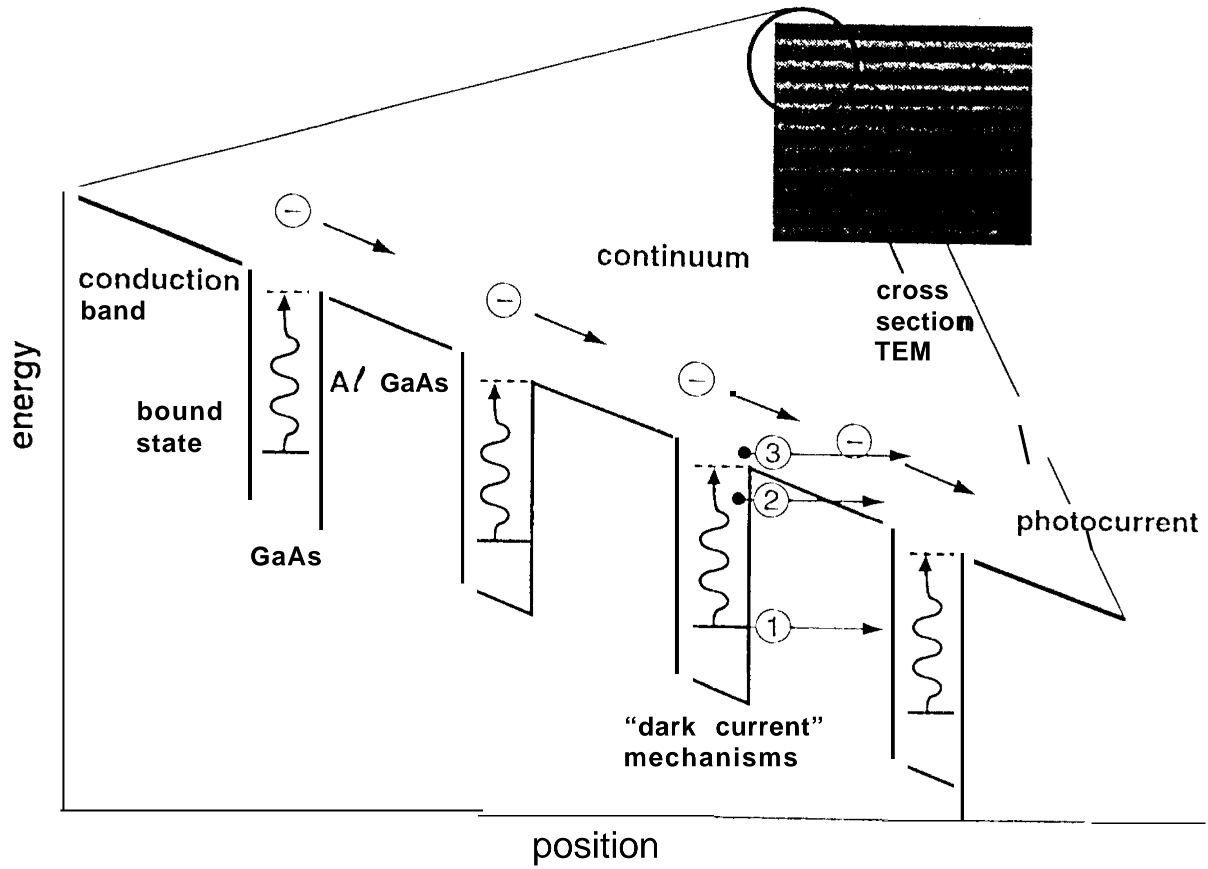
continuum
cross
section
TEM
conduction
band
A/ GaAs
bound
state
GaAs
energy
"dark current"
mechanisms
photocurrent
position
1
2
3

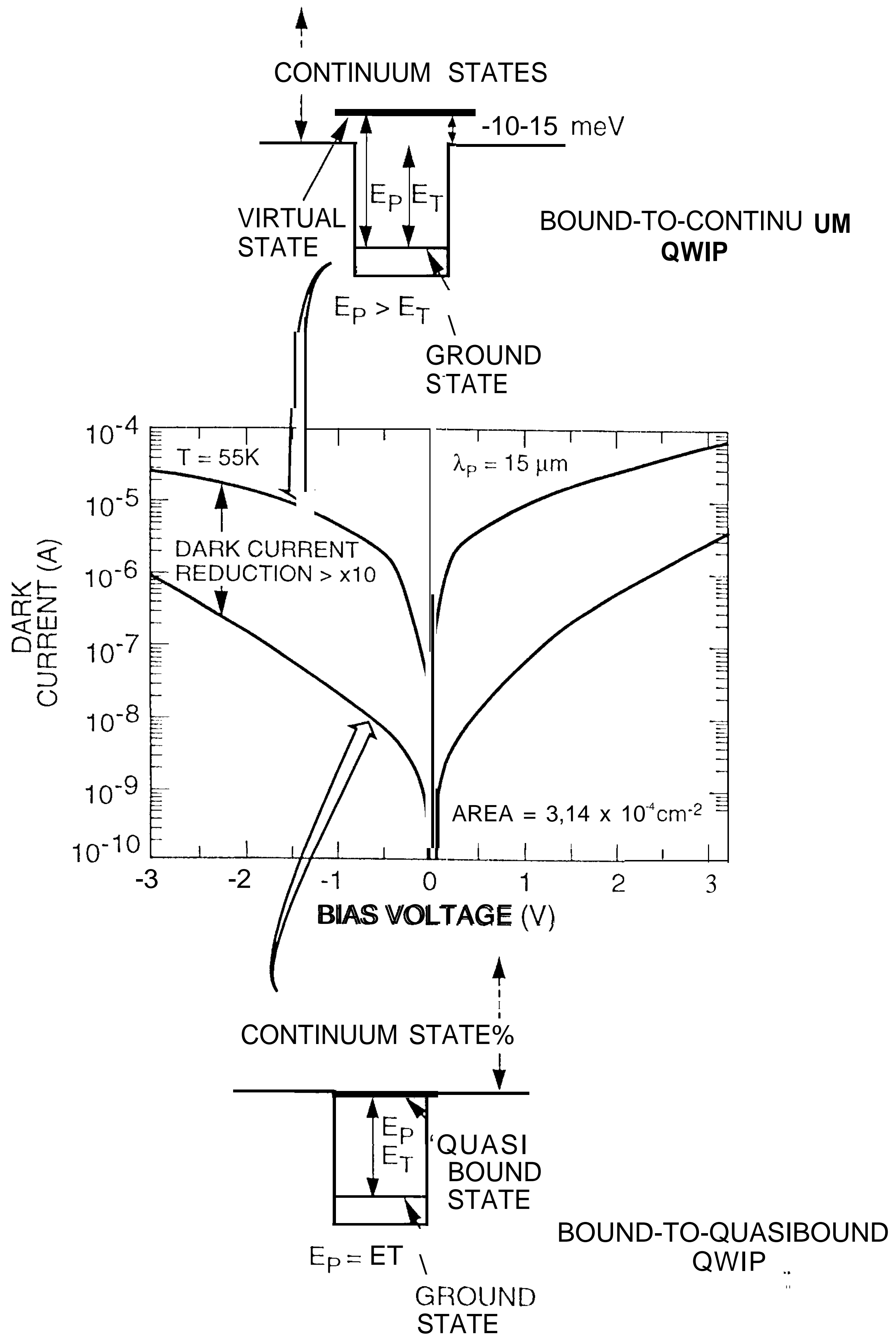

Fig. 2

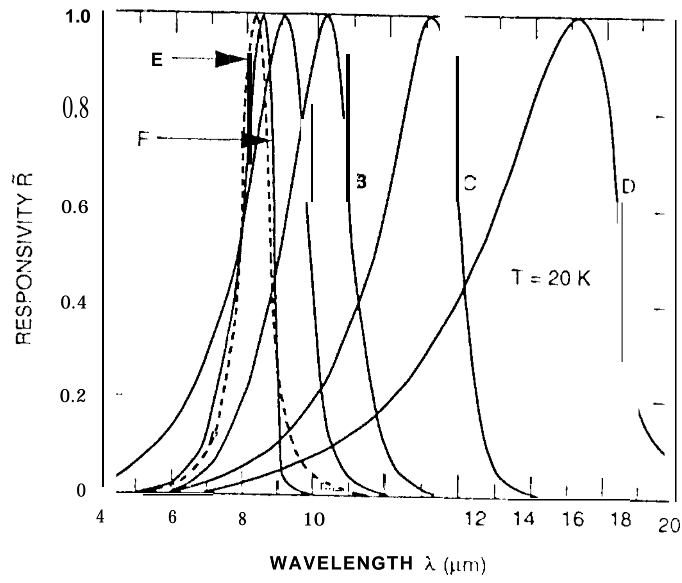
1.0
0.8
0.6
0.4
0.2
0
RESPONSIVITY R̃
E
F
B
C
D
T = 20 K
4
6
8
10
12
14
16
18
20
WAVELENGTH λ (μm)

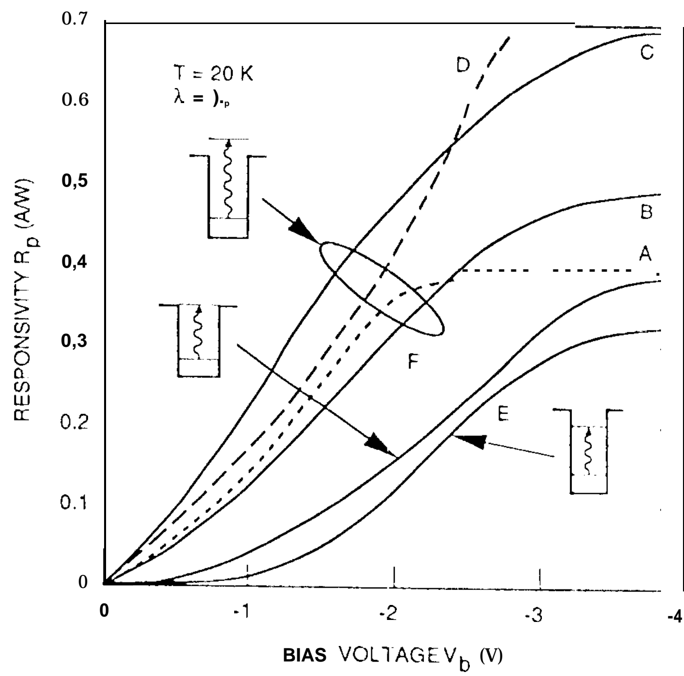
T = 20 K
RESPONSIVITY R_p (A/W)
BIAS VOLTAGE V_b (V)
A
B
C
D
E
F
0.7
0.6
0,5
0,4
0,3
0.2
0.1
0
-1
-2
-3
-4

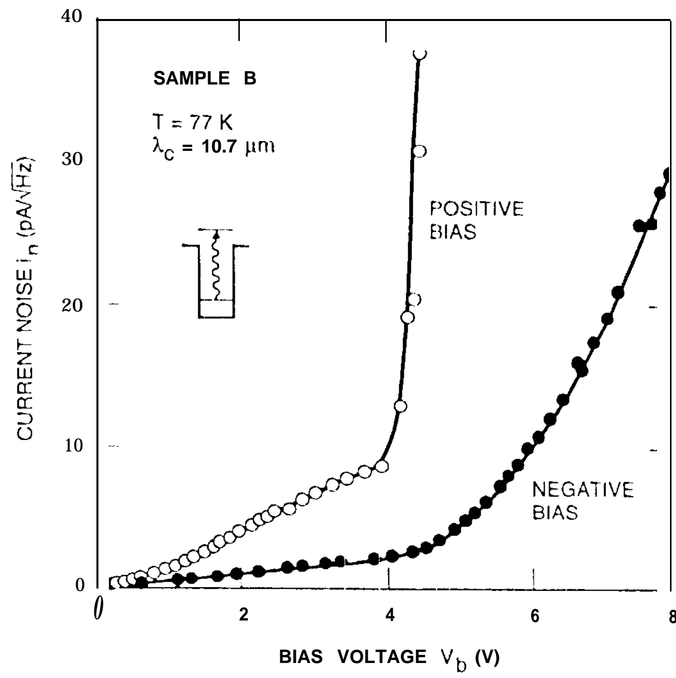
SAMPLE B
T = 77 K
λ_c = 10.7 μm
POSITIVE BIAS
NEGATIVE BIAS
CURRENT NOISE i_n (pA/√Hz)
BIAS VOLTAGE V_b (V)
0
10
20
30
40
0
2
4
6
8

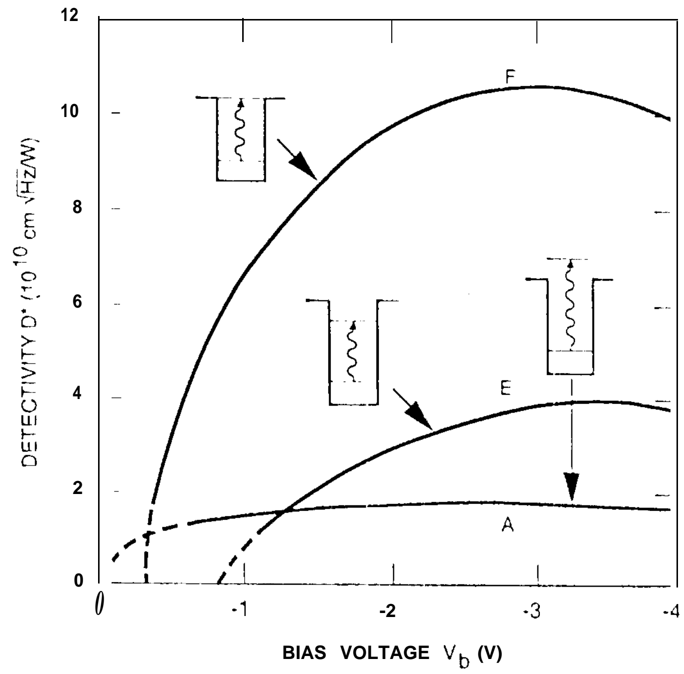

12
10
8
6
4
2
0
DETECTIVITY D* (10^10 cm √Hz/W)
F
E
A
0
-1
-2
-3
-4
BIAS VOLTAGE V_b (V)

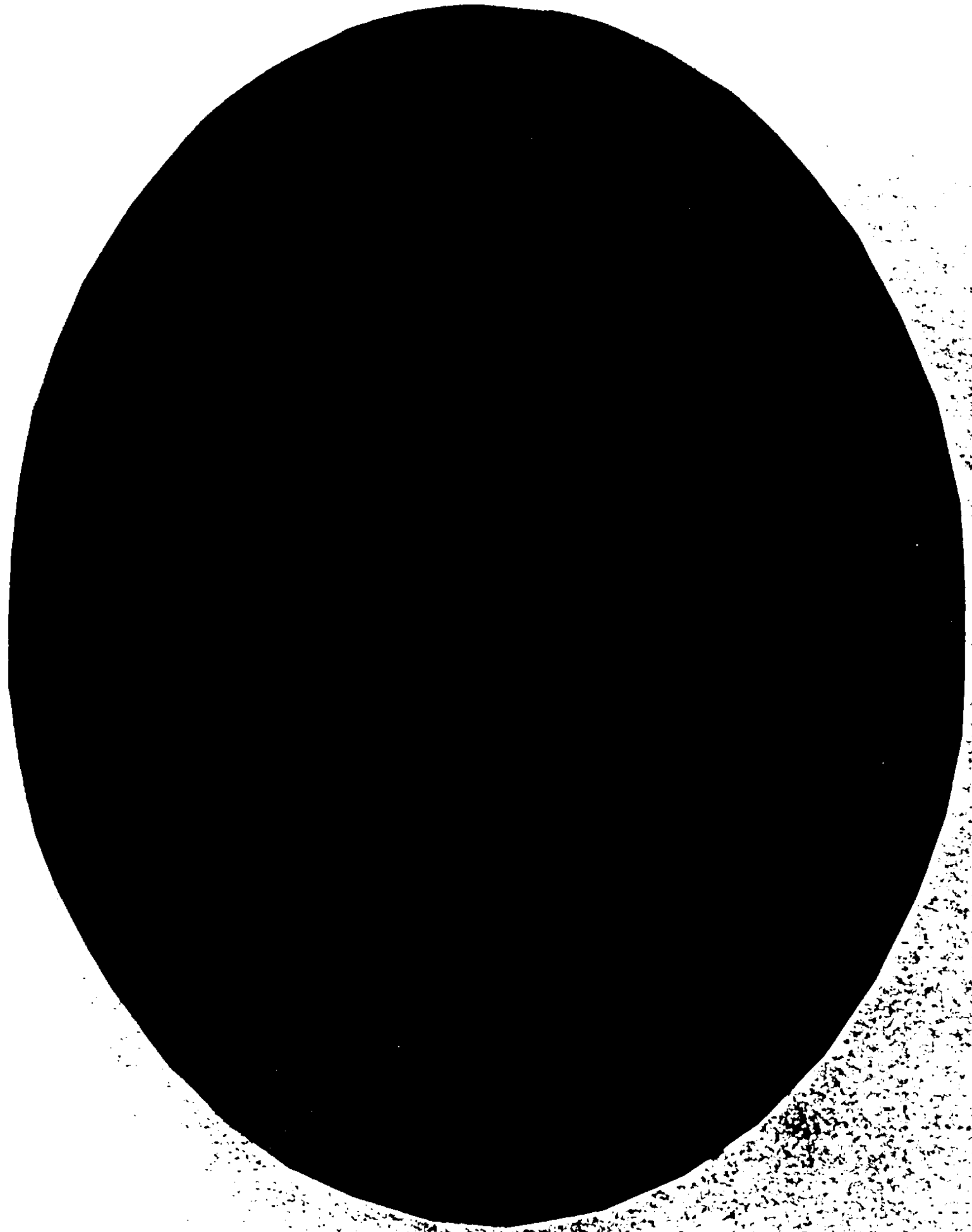

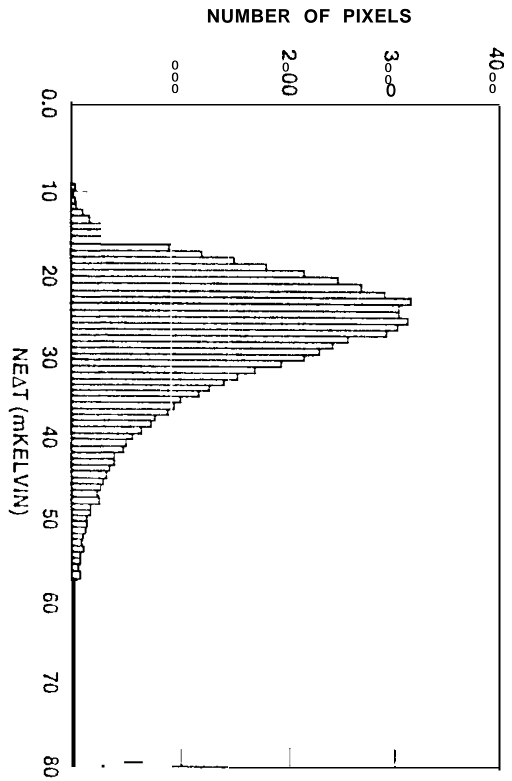
NUMBER OF PIXELS
NEΔT (mKELVIN)
0.0
10
20
30
40
50
60
70
80

TABLE I

RESPONSIVITY SPECTRAL PARAMETER FOR SAMPLES A-F

SAMPLE	λ_p (μm)	λ_c (μm)	$\Delta\lambda$ (μm)	$\Delta\lambda/\lambda$ (%)
A	8.95	9.8	2,25	25
B	9.8	10.7	2.0	20
c	13.2	14.0	2.5	19
D	16.6	19	4.6	28
E	8.1	8.5	0.8	10
F	8.4	8.9	0.9	11

NOTE: THESE PARAMETERS INCLUDE PEAK REPONSIVITY WAVELENGTH λ_p: LONG-WAVELENGTH CUTOFF λ_c: SPECTRAL WIDTH A?., AND FRACTIONAL SPECTRAL WIDTH $\Delta\lambda/\lambda$ (30).